ATTOSECOND PHYSICS

Soft x-ray excitonics

A. Moulet, J. B. Bertrand,* T. Klostermann, A. Guggenmos, N. Karpowicz, E. Goulielmakis†

The dynamic response of excitons in solids is central to modern condensed-phase physics, material sciences, and photonic technologies. However, study and control have hitherto been limited to photon energies lower than the fundamental band gap. Here we report application of attosecond soft x-ray and attosecond optical pulses to study the dynamics of core-excitons at the $L_{2,3}$ edge of Si in silicon dioxide (SiO_2). This attosecond x-ray absorption near-edge spectroscopy (AXANES) technique enables direct probing of the excitons' quasiparticle character, tracking of their subfemtosecond relaxation, the measurement of excitonic polarizability, and observation of dark core-excitonic states. Direct measurement and control of core-excitons in solids lay the foundation of x-ray excitonics.

In semiconductors, dielectrics, macromolecules, and clusters, electrons and holes form fundamental, hydrogen-like quasiparticles (excitons) that underlie a broad range of applications in photonics and electronics (*1*). Coherent ultrafast nonlinear spectroscopies (*2*) in the terahertz, infrared, and optical ranges (*3*) can now directly identify quasiparticles formed below the fundamental band gap of solids through observation of the excitonic optical Stark effect (*4*–*6*), Rabi oscillations (*7*), and Fano resonances (*8*). Access to essential physical properties of the excitons such as their polarizability (*9*) and relaxation time (*10*), as well as the presence of dark exciton states (*11*, *12*), lays the foundation of modern optical excitonics (*2*). Advancement of excitonic science and applications to the x-ray regime require the dynamic study of another class of quasiparticles that are formed between a core-hole in an atom of a solid and an excited electron generated by the absorption of x-rays (*13*). Ordinary absorption and photoelectron x-ray spectroscopies (*14*) can probe the core-hole excitation of solids, enabling a broad range of advances in condensed-phase physics (*15*), but fail to unambiguously identify quasiparticles in x-ray near-edge excitations (*16*–*21*) or to probe their dynamics. The establishment of x-ray excitonics calls for the advancement of coherent spectroscopy for dynamic study of core-excitons.

Previous ultrafast studies in the condensed phase have exploited the near-edge excitation of solids as ultrafast probes to study attosecond valence electron dynamics in dielectrics (*22*) and semiconductors (*23*), as well as intraband currents (*24*) induced by intense few-cycle laser pulses. Yet, the study of the dynamics and nonlinear properties of the electron volt–wide core-hole excitations in solids requires a probe with attosecond resolution.

Here we combine an attosecond soft x-ray pump pulse with an attosecond optical probe pulse to perform near-edge spectroscopy of solids and thereby observe the quasiparticle character and measure the relaxation dynamics, as well as the exciton-phonon coupling, the polarizability, and the effect of dark excitonic states.

Soft x-ray study of solids in the coherent regime can take advantage of already recognized dynamic signatures of excitonic phenomena in optical studies to probe the character (excitonic or nonexcitonic) of the near-edge structure. These include the optical Stark effect and dynamic exciton bleaching that are manifested in pump-probe measurements as a dynamic energy shift of absorption resonances (*4*, *5*) and an amplitude suppression (*3*, *25*), respectively. In pursuit of such excitonic signatures, we chose to study the $L_{2,3}$ edge of the silicon atom in silicon dioxide (SiO_2) (~100 to 110 eV) as a prototypical system. The excitonic nature of this edge has been a matter of controversy (*16*, *17*, *21*). Moreover, the Auger decay ensuing from excitation of the $L_{2,3}$ edge occurs on a time scale (*26*) commensurate with the characteristic frequency of optical phonons (*27*) or molecular vibrations excited by the attractive force of the core-hole to neighboring atoms, giving rise to many-body–dominated relaxation phenomena (*28*–*30*) that have hitherto remained inaccessible.

In our experimental scheme (Fig. 1 and supplementary text section 1), a soft x-ray ($E_{x\text{-}ray}$ ~105 eV) attosecond pulse (Fig. 1A, magenta beam and waveform) lasting approximately $\tau_{x\text{-}ray}$ ~ 200 as was used to excite the $L_{2,3}$ edge of Si in polycrystalline SiO_2 nanofilms (thickness ~125 nm). A representative absorption spectrum recorded by the apparatus is shown in Fig. 1B (blue line) and is juxtaposed with its high-resolution counterpart (red dashed line, Fig. 1B) acquired for the same samples at a synchrotron source (Physikalisch Technische Bundesanstalt, PTB). A and A′ in Fig. 1B mark near-edge absorption peaks, earlier identified as core-valence transitions from spin-orbit states of the 2p orbital of Si (*28*). A third, substantially broader (~1.8 eV) spectral peak—marked as B in Fig. 1B—is often attributed to transitions from the same 2p orbital to the conduction band of SiO_2 and is more rarely assigned an excitonic character (*17*, *28*).

To probe the coherent dynamics following the soft x-ray electronic excitation of the system in real time, an optical attosecond pulse (OAP) (peak field strength: F = 0.5 V/Å) (Fig. 1A, yellow line) (*31*) was used to dress the rapidly relaxing electric dipoles induced in the system by the soft-x ray attosecond pulse. We recorded transient absorption spectra as a function of the delay between the x-ray and optical pulse and composed transient absorption spectrograms for a delay range spanning several femtoseconds (Fig. 1C).

A close inspection of the transient absorption spectra in Fig. 1C permits the identification of excitonic signatures encoded in the dynamics of each absorption peak. The transient energy shift (dashed black line in Fig. 1C) of peaks A+A′ is a typical manifestation of the dynamic excitonic Stark effect (*5*, *6*, *25*, *32*), whereas the conspicuous, amplitude suppression of peak B is the dynamic signature of exciton bleaching (*25*). The notion of an exciton character of the near-edge x-ray excitation of Si in SiO_2 is further indicated by the monotonic increase in the energy shift of peaks A+A′ and the decrease in the amplitude of peak B as a function of the field strength of the optical attosecond probe (Fig. 1D) in analogy to earlier studies of these phenomena in optical excitons. The signatures of the excitonic character of the L-edge can also be recognized in the differential absorption spectra (Fig. 1E) by the formation of dispersive spectral profiles for the Stark effect (Fig. 1F) and the negative differential absorption for bleaching, respectively.

To associate our findings with the current understanding of electronic structure of the Si-$L_{2,3}$ edge in SiO_2 (*16*, *17*), we modeled the interaction of optical attosecond and soft x-ray pulses with SiO_2, as summarized in Fig. 2 and the supplementary text, using the semiconductor Bloch equations (SBEs) (*25*) on a basis of electronic states describing the near edges as calculated by density functional theory (DFT) simulations (fig. S1). The simulated density of states (DOS) (Fig. 2A) reveals that s-, p-, and d-like levels, as well as a dense continuum of states, practically dominate the Si-$L_{2,3}$ edge. Energetically, and in agreement with earlier studies, we can assign the A peaks to s-like excitons (red line), while peak B can be associated with d-like excitonic states (violet line). We accounted for the infinite effective mass of the 2p core level of Si by modeling it as a dispersion-free band (*33*). For simplicity, we modeled s states (peaks A and A′) as a single band (Fig. 2B). We introduced the continuum states into the model by the addition of a fourth band (green cloud). The excitonic character of the system was incorporated in our simulations by introducing Coulomb interactions to yield excitons (*25*) from each of the above bands (see also section 3 of the supplementary text).

The soft x-ray pulse drives transitions from the silicon 2p level to s and d excitons (violet arrows, Fig. 2B). Although p excitons (yellow line, Fig. 2A) contribute appreciably to the total state density of the system (Fig. 2A, blue line), their direct population from the 2p core is selection-rule prohibited, and thus they constitute dark excitonic

Max-Planck-Institut für Quantenoptik, Hans-Kopfermann-Str. 1, D-85748 Garching, Germany.
*Present address: Center for Optics, Photonics and Lasers (COPL), Universite Laval, 2375 de la Terrasse Street, G1V 0A6, Quebec, Canada. **†Corresponding author. Email: elgo@mpq.mpg.de**

states in the realm of ordinary x-ray $L_{2,3}$ edge spectroscopy. We show below that advancing x-ray spectroscopy into the coherent, nonlinear regime enables detection of these states.

Figure 2 shows representative absorption (Fig. 2C, black solid curve), as well as transient absorption spectrograms (Fig. 2C, color plot), simulated using optical and x-ray attosecond pulses identical to those in our experiments. Dephasing rates in the simulations were chosen to match the widths of peaks A and B in the unperturbed absorption spectra (Fig. 1B, solid line). The simulated spectrogram (Fig. 2C) qualitatively reproduces key features of the measured traces, including the Stark shift of peak A and the bleaching of peak B. Similar agreement is achieved by evaluating the differential absorption spectra, as shown in Fig. 2F.

The fair reproduction of the experimentally observed excitonic features by our simulations (Fig. 2, C and F) opens the possibility of exploring how these excitonic features emerge from specific interaction between the electronic states at the edge under the perturbative dressing of an optical field. The Stark effect dictates that a blue shift of s excitons (Figs. 1C and 2C) can only occur if the energy difference between these and higher excitonic states is lower than the photon energy of the optical field (~2 eV). A close inspection of the energy diagram in Fig. 2A suggests that only p states fulfill this prerequisite, as the coupling between s and d states is selection-rule prohibited. The exclusion of p states in our simulations does not influence the time-integrated (optical field–free) absorption spectra (black lines in Fig. 2, C and D); however, their exclusion prominently affects the dynamics encoded in the time-resolved trace (false color in Fig. 2, C and D) and results in the strong suppression of the energy shift on s excitons (Fig. 2D). This result suggests that the dark p-exciton states are primarily responsible for the Stark shift observed in s-exciton states and, as such, p states have become detectable in our time-resolved experiments.

Bleaching of d excitons (peak B in Figs. 1C and 2C), by contrast, is dominated by their resonant coupling with the excitonic continuum. Again, the exclusion of the state (green cloud, Fig. 2B) used to model the excitonic continuum in our simulation results in the elimination of the bleaching effects on the d-exciton peak.

Turning off the Coulomb interaction in our simulations (i.e., preventing exciton formation) reshapes the x-ray absorption edge, in agreement with previous numerical studies (*17*). More important, however, the elimination of the excitonic contributions again results in conspicuous changes to the dynamics (Fig. 2E), where the entire edge shows a weak but uniform blue shift. The observations in Fig. 2E are compatible with recent studies on the dynamic Franz-Keldysh effect (*24*), but do not reproduce the details of the experimental traces of our study. As a result, they further support the assignment of excitonic character to the Si $L_{2,3}$ edge in SiO_2.

On the basis of the above experiments and simulations, we have been able to acquire qualitative understanding on the physics of the Si $L_{2,3}$ absorption edge in SiO_2 and to ascertain the excitonic character of the resonant states, but quantitative physical information is still lacking. To gain access to this information, we undertook reconstruction of the recorded differential absorption spectrograms (Fig. 1E) and retrieved relevant physical quantities.

To this end, we modeled the absorption of soft x-rays in solids directly in the time domain. The electronic dipole $d_x(t)$ induced by the absorption of the x-ray pulse (*29*, *34*) can be expressed as $d_x(t) \propto \theta(t) e^{-\omega_e t} e^{\frac{\Gamma}{2\hbar}t} e^{\phi(t)}$ where ω_e is the transition energy with respect to the core level (2p), $\Gamma/\hbar$ represents the inverse Auger lifetime of the core-hole of Si, t is time, and $\theta(t)$ is the Heaviside function. The first three terms describe free induction decay of the excited dipoles characteristic for atomic systems, resulting in Lorentzian line shapes in the spectral domain. $\phi(t)$ accounts for many-body relaxation dynamics resulting from scattering of the exciton with longitudinal optical (LO) phonons. The latter are created by the attractive (*35*) force of the core-hole to electrons in nearest-neighbor atoms resulting in the structural rearrangement of the system and can be expressed as (*29*)

$$\phi(t) = (M_0^2/\omega_0^2)((2N+1)(1-\cos(\omega_0 t)) - i(\omega_0 t - \sin(\omega_0 t)) \quad (1)$$

Here ω_0 is the energy of the LO phonon in SiO_2, M_0 is the linear coupling strength between phonons and the excited electronic dipole, and N is the thermal phonon population (*29*). For SiO_2, the dominant LO phonon oscillations occur at $\frac{2\pi}{\omega_0}$ ~ 27 fs (*27*), and the Auger decay of the Si 2p core hole has been assigned a value of $\hbar\Gamma_{\mathrm{Auger}}^{-1}$ ~ 15 fs on the basis of ordinary linewidth measurements (*26*). The validity of inferring the decay time of the core-hole from that of

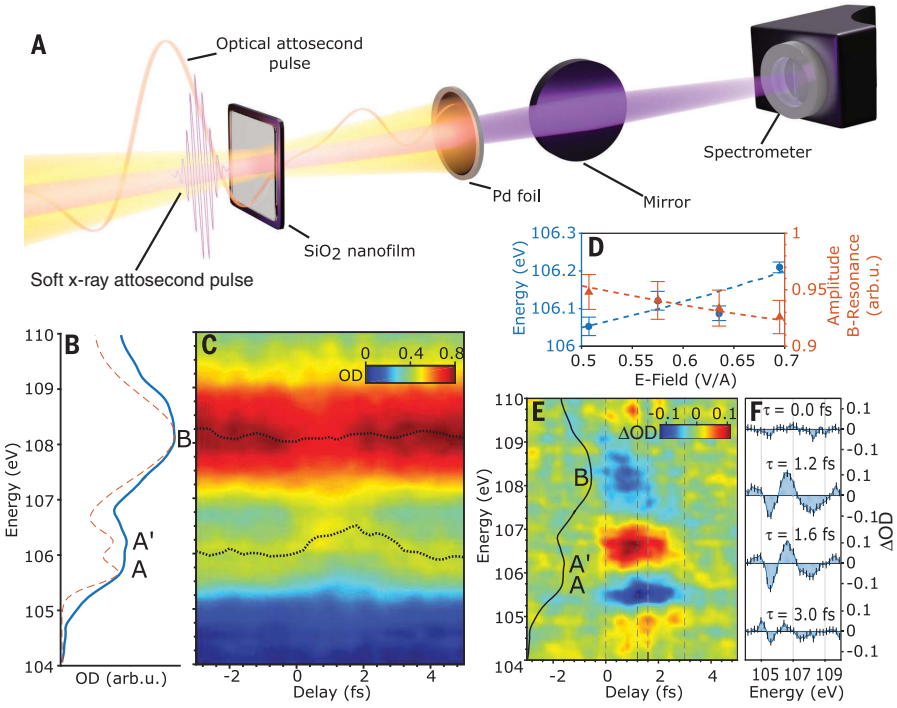

Fig. 1. Attosecond, real-time tracking of Si $L_{2,3}$ core-hole dynamics. (**A**) Experimental setup: Soft x-ray attosecond pulses are used to excite the Si $L_{2,3}$ edge in thin SiO_2 nanofilms (125 nm). An optical attosecond probe pulse (half-cycle FWHM duration ~350 as) coherently perturbs the induced x-ray dipoles, the spectra of which are recorded by a spectrometer placed downstream of the sample upon reflection off a rhodium mirror. A Pd metal nanofoil provides high-pass transmission and optical radiation blocking. (**B**) $L_{2,3}$ spectra of Si in polycrystalline SiO_2 (blue line) recorded by the spectrometer (resolution ~350 meV) along with corresponding spectra of the same samples acquired at a synchrotron source (PTB) (red dashed line). (**C**) Transient absorption spectra (averaged over three consecutive measurements performed under identical conditions) of the silicon edge recorded as a function of the delay (step size 200 as) between soft x-ray and optical fields. The color scale represents optical density (OD). (**D**) Dependence of the energy shift of A peaks (blue dots) and amplitude of peak B (red dots) versus optical field strength for a fixed delay (τ = 0.5 fs) between optical and soft x-ray pulses. Dashed lines are simulations based on the reconstruction model discussed in the text. (**E**) Differential transient absorption spectrograms derived from the data in (C). Differential absorption is defined as the difference in absorption of the x-ray pulse in the presence and the absence of the optical field. (**F**) Representative spectra at selective delays in (E) reveal the buildup and disappearance of dispersive spectral profiles. Error bars indicate the standard deviation of the mean values acquired from three consecutive measurements.

isolated atoms from spectral measurements has been earlier verified by time-resolved measurements (*36*).

To account for the effect of the optical field on the dynamics of the system, the electronic dipole induced in the system by soft x-ray and optical attosecond pulse can be expressed (*34*) as $d_x(t) \propto \theta(t) e^{-i\omega_e t} e^{-\frac{\Gamma}{2\hbar}t} e^{\phi(t)} e^{\phi_L(t,\tau)}$ where

$$\phi_L(t,\tau) = -i\frac{\alpha}{2}\int_0^t E^2(t'-\tau)dt' - \gamma\int_0^t E^2(t'-\tau)dt' \quad (2)$$

is an optical gate.

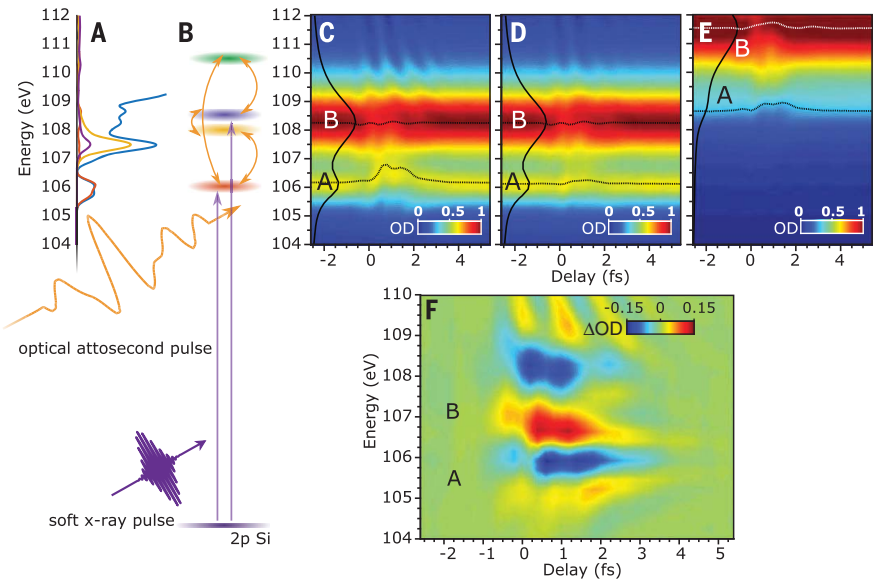

Fig. 2. Theoretical modeling of soft x-ray excitonic phenomena. (**A**) Density of states (DOS) of the Si $L_{2,3}$ edge in SiO_2 evaluated by DFT simulations. S (red line), p (yellow line), and d states (violet line) dominate the near-edge absorption. Blue line marks the total DOS. (**B**) Interaction scheme. The attosecond soft x-ray pulse drives transitions (violet arrows) from the 2p level of Si to s (red) and d (violet) states of the Si edge in SiO_2. The excitonic continuum is modeled by a single band (green cloud). The p states are marked by a yellow cloud. The field of the optical attosecond pulse in turn dresses the excited system. (**C**) Transient absorption spectra as a function of the delay between optical and soft x-ray fields. A and B mark the peaks. Dashed lines in A and B mark the central energy of the peaks A and B in accordance with the experiments. Bare soft x-ray absorption predicted by the model is shown as a solid black curve. (**D**) As in (C) but excluding p states in the model. (**E**) As in (C) but excluding excitonic effects. (**F**) Differential transient absorption spectra as a function of the delay between optical and x-ray field for the data in (C).

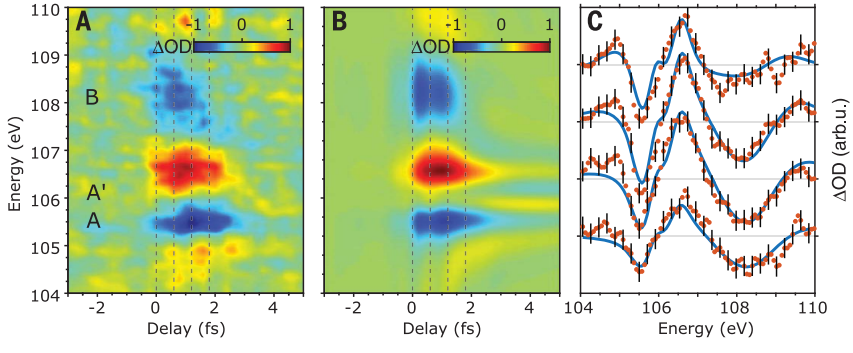

Fig. 3. Retrieval of soft x-ray–induced core-exciton dynamics in SiO_2. (**A**) Measured (also in Fig. 1E) differential absorption spectrogram as a function of the delay between soft x-ray and optical attosecond pulses. (**B**) Reconstructed spectrogram based on the model summarized in the text. (**C**) Measured (red dots) and reconstructed (blue line) differential transient absorption spectra for representative delays (τ = 0, 0.6, 1.2, and 1.8 fs; indicated by the thin dashed line, from bottom to top) are juxtaposed for comparison. Error bars (shown for every third data point for clarity) indicate the standard deviation of the mean value from three measurements acquired under identical conditions.

Here τ is the delay between pump and probe fields, α is the polarizability, and γ accounts for amplitude reduction resulting from the optical field–induced coupling of the soft x-ray dipole with nearby electronic states (more detail on the reconstruction model is given in the supplementary text). We have verified that our model accurately describes nonlinearities in our experiments by testing its capability to reproduce the field-dependent shift of peaks A and A′ and the amplitude damping of peak B for a range of optical field strengths, as indicated by the dashed lines in Fig. 1D.

Figure 3 shows the experimental differential absorption spectrogram (Fig. 3A) and its reconstruction (Fig. 3B) based on the above-described model. The high fidelity of the reconstruction is underlined by the direct comparison of measured (Fig. 3C, red points) and reconstructed (Fig. 3C, blue lines) differential spectra at indicated (dashed lines in Fig. 3, A and B) representative delays. Figure 4A shows the unperturbed relaxation profiles of s and d excitons retrieved from the reconstruction in Fig. 3. S excitons (red and blue curves in Fig. 4A) relax over a time interval of $T_A = 3.2 \pm 0.3$ fs; $T_{A'} = 2.3 \pm 0.2$ fs ($\hbar\Gamma_A^{-1} = 5.3 \pm 0.3$ fs; $\hbar\Gamma_{A'}^{-1} = 3.8 \pm 0.2$ fs) and d excitons (violet curve, Fig. 4A), within $T_B = 0.75 \pm 0.04$ fs ($\hbar\Gamma_B^{-1} = 1.25 \pm 0.04$ fs), measured at the full width at half maximum (FWHM) (and $1/e$) of the intensity profile. Nevertheless, more important than directly accessing the fastest electronic relaxation dynamics to date is the capability of our approach for tracking physical properties of the system within these brief time intervals during which the interaction remains coherent. The considerably shorter relaxation times of d excitons (peak B) with respect to s excitons (peaks A and A′) result from a stronger coupling of these excitons with optical phonons. Indeed, the coupling strengths of exciton and LO phonon retrieved for s excitons is $M_A = 0.158 \pm 0.006$ eV; $M_{A'} = 0.228 \pm 0.009$ eV, whereas $M_B = 0.724 \pm 0.02$ eV is the coupling of the optical phonon with d excitons. The former agrees with earlier spectral domain estimations for the A and A′ peaks (s excitons), which predicted $M_{A/A'} < 1$ eV (*28*). This result is also compatible with the larger Bohr radius of d excitons compared to s excitons as revealed by our density functional theory (DFT) simulations (fig. S2), implying a wider phase space contributing to dephasing of d excitons.

Figure 4, B to D, contrast the optical field–free relaxation of the s and d excitons (dashed lines) with those dynamically gated by the optical field, as retrieved in our reconstruction for a delay of τ = 0.5 fs between x-ray and optical pulses (solid lines). The optical attosecond pulse (yellow line) gates the dipole of s excitons by introducing a sizable phase shift [$\Delta\phi = 0.2\pi$ rad] (red line), which is compatible with the prominent shift of the A peaks shown in our time-resolved traces (Fig. 1C) and simulations (Fig. 2C). The corresponding polarizability retrieved is $\alpha_A = 3.6 \pm 0.2$ eV Å^2 V^{-2}; $\alpha_{A'} = 3.55 \pm 0.09$ eV Å^2 V^{-2}, and the amplitude damping is $d_A = 0.17 \pm 0.01$; $d_{A'} = 0.00 \pm 0.03$ $\left(\text{where } d_i = \exp\left[-\gamma_i\int_{-\infty}^{\infty} E^2(t)dt\right]\right)$. By contrast,

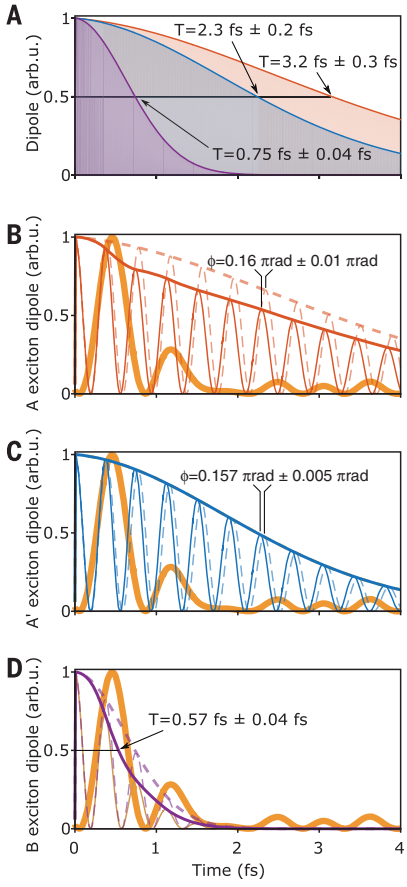

Fig. 4. Tracking and controlling the core-exciton relaxation. (**A**) Retrieved relaxation dynamics for s excitons (red and blue lines) (corresponding also to peaks A and A′ of Fig. 1B) and d excitons (violet line) (peak B of Fig. 1B). (**B**) Retrieved gated dynamics of s excitons (A) (red line) for a relative delay (τ = 0.5 fs) between soft x-ray pulse and optical gate (yellow line). Dashed line indicates the optical field–free relaxation of the s exciton. (**C**) Retrieved gated dynamics of s excitons (A′) (blue line) for a relative delay (τ = 0.5 fs) between soft x-ray pulse and optical gate (yellow line). (**D**) Retrieved gated dynamics of d excitons (B) (violet line) for a relative delay (τ = 0.5 fs) between soft x-ray pulse and optical gate (yellow line). Dashed lines indicate the optical field–free relaxation of the d exciton. The transition frequency has been downscaled to improve visibility of the oscillation and phase shift.

gating d excitons (violet line, Fig. 4D) reveals a weak polarizability $\alpha_B = 0.07 \pm 0.06$ eV Å^2 V^{-2} but a strong amplitude damping $d_B = 0.40 \pm 0.01$. The latter implies that the optical field acts primarily as an amplitude gate (compatible also with the observation of Figs. 1C and 2C) and results in the effective shortening of the relaxation time of the d exciton down to ~ 500 as. Note that owing to the nonlinearity underlying the interaction (see fig. S4 for different delay settings), the gating and control action of the optical field is restricted to the ~350-as time window of the most intense optical half cycle of the gate pulse.

We repeated the reconstruction with an extended alternative model (see supplementary text 4.2) to access the energy of the p exciton and the dipole matrix elements μ coupling it to the other excitons. We could retrieve an energy value of the dark-exciton state of $E_p = 107.2 \pm 0.2$ eV, which is in good agreement with the predictions of the DFT simulation (Fig. 2A) (E_p ~ 107.8 eV) as well as estimations derived via multi-edge x-ray spectroscopies (*37*). The evaluated matrix elements linking s and p excitons are $\mu_{Ap} = 1.5 \pm 0.2$ atomic units (au); $\mu_{A'p} = 2.9 \pm 0.5$ au and $\mu_{Bp} = 0.7 \pm 0.2$ au, respectively. The above data represent the complete characterization of the dark excitonic state and allow further estimations for the s-ground state of the core exciton. The nonresonant polarizability can be estimated as $\alpha \sim \mu_{sp}^2/\Delta E_{sp}$, yielding a value of $\alpha_A \sim 40$ au; $\alpha_{A'} \sim 233$ au. For a hydrogenic system, the nonresonant polarizability α and the Bohr radius r_B are linked in atomic units as $\alpha = \frac{9}{2}\varepsilon r_{B,exc}^3$, where ε is the dielectric constant of SiO_2. The evaluation of the Bohr radius yields $r_{B,exc}^{(A)} \sim 1.3a_B$; $r_{B,exc}^{(A')} \sim 2.4a_B$, where a_B is the Bohr radius of the hydrogen atom. These results are in very good agreement with the radius of the s exciton evaluated by our DFT simulations $r_B(\text{theory}) \sim 1.3a_B$ and suggest that our approach can probe the extreme confinement of the core-exciton within sub–unit-cell (for SiO_2 ~ 5 Å) dimensions directly from dynamic measurements.

This capability of probing ultrafast dephasing of excited electrons in bulk solids may also prove essential for understanding the role of dephasing in emerging photonic phenomena such as high harmonic generation in such media (*38*). Precise knowledge of the polarizability of core excitons is an essential prerequisite for porting optical excitonic control of radiation (*39*) into the x-ray regime and realizing sub–optical cycle gates of x-ray radiation, an unexplored possibility of critical importance in free electron laser (FEL) technologies and their applications.

REFERENCES AND NOTES

1. G. D. Scholes, G. Rumbles, *Nat. Mater.* **5**, 683–696 (2006).
2. S. W. Koch, M. Kira, G. Khitrova, H. M. Gibbs, *Nat. Mater.* **5**, 523–531 (2006).
3. S. T. Cundiff, *Opt. Express* **16**, 4639–4664 (2008).
4. W. H. Knox, D. S. Chemla, D. A. B. Miller, J. B. Stark, S. Schmitt-Rink, *Phys. Rev. Lett.* **62**, 1189–1192 (1989).
5. T. Unold, K. Mueller, C. Lienau, T. Elsaesser, A. D. Wieck, *Phys. Rev. Lett.* **92**, 157401 (2004).
6. A. Mysyrowicz *et al.*, *Phys. Rev. Lett.* **56**, 2748–2751 (1986).
7. A. Zrenner *et al.*, *Nature* **418**, 612–614 (2002).
8. U. Siegner, M. Mycek, S. Glutsch, D. S. Chemla, *Phys. Rev. Lett.* **74**, 470–473 (1995).
9. F. Wang *et al.*, *Nat. Mater.* **5**, 861–864 (2006).
10. L. Schultheis, J. Kuhl, A. Honold, C. W. Tu, *Phys. Rev. Lett.* **57**, 1797–1800 (1986).
11. Z. Ye *et al.*, *Nature* **513**, 214–218 (2014).
12. C. Poellmann *et al.*, *Nat. Mater.* **14**, 889–893 (2015).
13. S. T. Pantelides, *Phys. Rev. B* **11**, 2391–2411 (1975).
14. F. de Groot, A. Kotani, *Core Level Spectroscopy of Solids* (CRC Press, 2008).
15. D. C. Koningsberger, R. Prins, *X-ray Absorption: Principles, Applications, Techniques of EXAFS, SEXAFS, and XANES* (Wiley, 1987).
16. R. Buczko, G. Duscher, S. J. Pennycook, S. T. Pantelides, *Phys. Rev. Lett.* **85**, 2168–2171 (2000).
17. G. Duscher, R. Buczko, S. J. Pennycook, S. T. Pantelides, *Ultramicroscopy* **86**, 355–362 (2001).
18. A. Zunger, *Phys. Rev. Lett.* **50**, 1215–1218 (1983).
19. S. Nufer, T. Gemming, C. Elsässer, S. Köstlmeier, M. Rühle, *Ultramicroscopy* **86**, 339–342 (2001).
20. F. C. Brown, C. Gähwiller, A. B. Kunz, N. O. Lipari, *Phys. Rev. Lett.* **25**, 927–930 (1970).
21. L. A. J. Garvie *et al.*, *Am. Mineral.* **85**, 732–738 (2000).
22. M. Schultze *et al.*, *Nature* **493**, 75–78 (2013).
23. M. Schultze *et al.*, *Science* **346**, 1348–1352 (2014).
24. M. Lucchini *et al.*, *Science* **353**, 916–919 (2016).
25. H. Haug, S. W. Koch, *Quantum Theory of the Optical and Electronic Properties of Semiconductors* (World Scientific, ed. 5, 2009).
26. J. D. Bozek, G. M. Bancroft, J. N. Cutler, K. H. Tan, *Phys. Rev. Lett.* **65**, 2757–2760 (1990).
27. F. L. Galeener, G. Lucovsky, *Phys. Rev. Lett.* **37**, 1474–1478 (1976).
28. W. L. O'Brien *et al.*, *Phys. Rev. B condens. Matter* **47**, 140–143 (1993).
29. G. D. Mahan, *Phys. Rev. B* **15**, 4587–4595 (1977).
30. C.-O. Almbladh, *Solid State Commun.* **22**, 339–342 (1977).
31. M. T. Hassan *et al.*, *Nature* **530**, 66–70 (2016).
32. M. Kira, S. W. Koch, *Semiconductor Quantum Optics* (Cambridge Univ. Press, 2011).
33. F. Bassani, *Appl. Opt.* **19**, 4093–4100 (1980).
34. A. Wirth *et al.*, *Science* **334**, 195–200 (2011).
35. R. D. Carson, S. E. Schnatterly, *Phys. Rev. B Condens. Matter* **39**, 1659–1662 (1989).
36. M. Drescher *et al.*, *Nature* **419**, 803–807 (2002).
37. D. Li *et al.*, *Am. Mineral.* **79**, 785–788 (1994).
38. M. Garg *et al.*, *Nature* **538**, 359–363 (2016).
39. G. Günter *et al.*, *Nature* **458**, 178–181 (2009).

ACKNOWLEDGMENTS

This work was supported by a European Research Council grant (Attoelectronics-258501), the Deutsche Forschungsgemeinschaft Cluster of Excellence, Munich Centre for Advanced Photonics, the Max Planck Society, and the European Research Training Network (MEDEA-641789). J.B.B. acknowledges a Banting Postdoctoral Fellowship from the Natural Sciences and Engineering Research Council (NSERC). The data are available from E.G. upon request.

SUPPLEMENTARY MATERIALS

www.sciencemag.org/content/357/6356/1134/suppl/DC1
Materials and Methods
Figs. S1 to S4
References (*40*–*57*)

25 April 2017; accepted 22 August 2017
10.1126/science.aan4737

Soft x-ray excitonics

A. Moulet, J. B. Bertrand, T. Klostermann, A. Guggenmos, N. Karpowicz and E. Goulielmakis

Science **357** (6356), 1134-1138.
DOI: 10.1126/science.aan4737

A quick glimpse of the x-ray aftermath

X-rays pass through your skin to reveal the inner workings below. At the atomic scale, x-rays skip past valence electrons to grab hold of the core electrons closer to the nucleus. Moulet *et al.* used two successive, extremely short laser pulses (lasting less than a quadrillionth of a second) to initiate and then track this process in a sample of silica. This study uncovered the angular momentum character and relaxation dynamics of the excitons, or electron-hole pairs, ensuing from the x-ray absorption.

Science, this issue p. 1134